Photocatalytic Hydrodechlorination of Trace Carbon Tetrachloride (CCl_4) in Aqueous Medium

ARTICLE *in* INDUSTRIAL & ENGINEERING CHEMISTRY RESEARCH · MAY 2014

Impact Factor: 2.59 · DOI: 10.1021/ie500344v

I&EC research
Industrial & Engineering Chemistry Research

Article

pubs.acs.org/IECR

Photocatalytic Hydrodechlorination of Trace Carbon Tetrachloride (CCl_4) in Aqueous Medium

William K. O'Keefe,*[,†] Yin Liu,[‡] Michael R. Sasges,[†] Michael S. Wong,[§] Han Fu,[∥] Tsuyoshi Takata,[∥] and Kazunari Domen[∥]

[†]Advanced Technology Team, Trojan Technologies, 3020 Gore Road, London, Ontario, Canada N5 V 4T7

[‡]Department of Chemical and Biological Engineering, Western University, London, Ontario, Canada N6A 5B9

[§]Department of Chemical and Biological Engineering, Rice University, Houston, Texas 77251-1892, United States

[∥]Department of Chemical System Engineering, The University of Tokyo, 7-3-1 Bunkyo-ku, Tokyo, Japan 113-8656

Supporting Information

ABSTRACT: The technical feasibility of the photocatalytic hydrodechlorination of CCl_4 utilizing H_2 produced in situ from photocatalytic water splitting was investigated using multifunctional Pd−NiO/$NaTaO_3$:La catalysts and a O/$NaTaO_3$:La + Pd−Au/IX (ion-exchange resin) mixture-of-catalysts approach. In the former case, the incorporation of Pd into the water-splitting photocatalyst resulted in the reduction of H_2 evolution by 3 orders of magnitude. However, the multifunctional catalyst exhibited a remarkable activity for CCl_4 removal. The important catalyst parameters were elucidated by the response surface methodology. The Ni and Pd loadings and the catalyst reduction temperature had significant, nonlinear effects on the catalyst activity, indicating that both NiO and Pd nanoparticles play important roles in the photocatalytic hydrodechlorination of CCl_4. The strong dependence of the turnover frequency on the catalyst parameters that govern the dispersion of the catalytic phases implies that the reaction is structure-sensitive.

INTRODUCTION

Rapid population growth and the increased usage of personal care products and pharmaceutically active compounds, combined with unrelenting industrialization, are resulting in the contamination of drinking water resources and an increasing demand for potable water. It has been suggested that, by 2025, 1.8 billion people could be living under conditions of absolute water scarcity and two-thirds of the world's population could be living under conditions of water stress.[1] Many emerging micropollutants found in drinking water sources, such as pesticides, pharmaceuticals, and personal care products, cannot be effectively removed by conventional water treatment processes. Some micropollutants, such as perchlorate and carbon tetrachloride (CCl_4), cannot be effectively treated by advance oxidation processes, such as ozonation and UV/H_2O_2 treatment. Moreover, the hydroxyl radical chemistries afforded by these technologies are indiscriminate, resulting in uncontrolled and sometimes undesirable byproduct distributions that must be addressed and requiring further downstream quenching of some species of unreacted oxidants.

In this work, a novel photocatalytic process that enables the treatment of recalcitrant micropollutants by reductive chemistry, utilizing H_2 produced in situ from photocatalytic water splitting, is investigated.[2] The in situ H_2 can be utilized to effect catalytic hydrogenolysis, hydrodehalogenation, and hydrogenation. In addition, the photoexcited electrons can react directly with adsorbed contaminants, leading to their catalytic reduction. This green chemistry does not require the handling and addition of chemical reagents, nor does it require downstream quenching, and it can be conducted with chemical control and high selectivity. The chemistry is enabled by UV-active photocatalysts with quantum efficiencies much greater than those associated with UV/TiO_2 advanced oxidation processes.[3] Thus, photocatalytic reduction as a water treatment technology potentially affords alternative routes through kinetically facile and thermodynamically favorable pathways to stable, lower-energy products that are substantially less toxic than the parent compounds.

The mechanism of photocatalytic reduction follows several elementary steps.[3] First, the absorption of UV light by the semiconductor results in the generation of photoexcited electrons and holes. The holes migrate to surface sites where their interaction with adsorbed water results in its oxidation, causing oxygen evolution and the creation of protons. The protons migrate to the active sites of the cocatalyst, where they recombine with the photoexcited electrons to produce hydrogen. The surface mobile hydrogen atoms migrate to catalyst active sites, where the contaminants adsorb and react with hydrogen to form the desired product.[2] Two distinct approaches are proposed (Scheme 1) to facilitate the photocatalytic reduction of contaminants. The first utilizes a multifunctional catalyst to facilitate all of the chemistry on a single surface, and the second utilizes two kinds of catalysts, one of which provides the reactant H_2 from photocatalytic water splitting while the other enables the catalytic reduction of the contaminant by reaction with H_2.[2,4]

Received: January 27, 2014
Revised: April 28, 2014
Accepted: May 17, 2014
Published: May 28, 2014

dx.doi.org/10.1021/ie500344v | Ind. Eng. Chem. Res. 2014, 53, 9600−9607

Scheme 1. Schematic Representations of the Photocatalytic Reduction of Contaminants Utilizing (left) the Multifunctional Catalyst Approach and (right) the Mixture-of-Catalysts Approach[a]

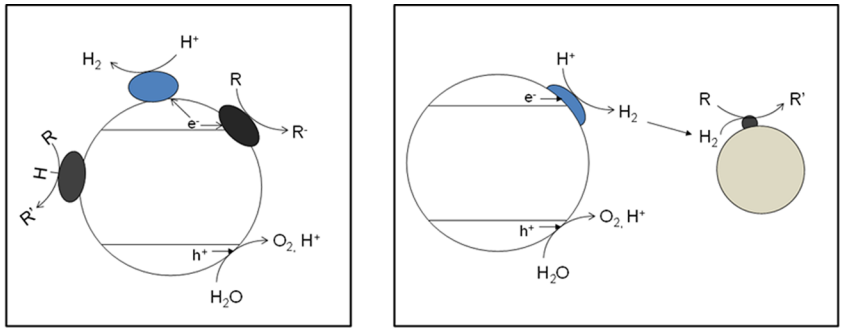

[a]Photocatalyst indicated in white, NiO nanoparticles in blue, dispersed metal catalyst in dark gray, and conventional hydrogenation catalyst support in light gray.

The mixture-of-catalysts approach has the advantage that the light-dependent and light-independent reactions are decoupled. The water-splitting catalyst can be engineered and optimized independently from the reduction catalyst. Similarly, the catalyst zones in a reactor can be engineered independently as well, providing more flexibility to the reactor designer. The multifunctional catalyst approach has the advantage that the reactant H_2 is created at the catalyst surface where it is needed to effect catalytic reduction. Thus, internal and external mass-transfer limitations, which might be significant because of the sparing solubility of H_2 in water, can be avoided. Consequently, the H_2 and energy input can be utilized more efficiently. Experiments were conducted to evaluate the technical feasibility of the photocatalytic hydrodechlorination of CCl_4 considering these two approaches.

CCl_4 was selected as the model compound for investigation because it is a challenging substrate that cannot be degraded by UV photolysis and is not readily treatable by advanced oxidation processes. The photocatalytic removal of CCl_4 and other chlorinated compounds from water has been investigated previously. However, the catalysts investigated in these earlier studies exploited free-radical mechanisms involving the reaction of CCl_4 and conduction-band electrons rather than the direct reaction of hydrogen with CCl_4.[5−8] Much research has been conducted investigating TiO_2 and dye-sensitized TiO_2 to effect the removal of chlorinated compounds in water.[5] Recently, novel catalysts were reported for the photocatalytic removal of CCl_4 from water including Zr/MCM-41 and N-doped graphene P-25.[6,7] However, the activities of these catalysts remain relatively low, with about 40% and 80% conversions of CCl_4 after 1 h reported in the studies using Zr/MCM-41 and N-doped graphene P-25, respectively. Consequently, there remains incentive to develop novel and improved photocatalysts for CCl_4 removal in aqueous systems.

EXPERIMENTAL SECTION

A flat-bottomed, 1 L, jacketed stirred tank reactor constructed of Momentive 214 fused silica equipped with a 4-in. × 4-in. stainless steel baffle kit and agitated with 45° and 60° pitched-blade impellers in the water and the reactor headspace, respectively, was affixed immediately above the collimator of a custom mercury amalgam UV light source. The UV source was previously characterized and found to deliver an average irradiance of 36.4 mW/cm^2 and a total power of 2.48 W at 254 nm. The agitation rate was controlled by an Optichem Tempstir proportional−integral−derivative (PID) controller. The reactor temperature was controlled indirectly by the reactor jacket temperature, which was controlled using a Thermoscientific RTE7 heater/chiller. The photoreactor was coupled with an Agilent Technologies 7890A gas chromatograph. Ultra-high-purity (UHP) N_2 (Praxair, 5.0) was used as the carrier gas to remove the evolved gases from the reactor headspace for online gas chromatography/thermal conductivity detector (GC/TCD) analysis. The N_2 feed to the reactor was controlled and monitored using a Brooks Instruments 0254 digital mass flow controller. The effluent was monitored using a Sierra 830 digital mass flow meter, to close the mass balance. The effluent passed through a multiport valve with a 1 mL sample loop with a load time of 30 s and an injection time of 30 s into a 30 m × 0.25 mm × 0.25 μm narrow-bore HP-Molesieve capillary column (Agilent J&W) with an isothermal oven profile of 40 °C for 4.6 min at a carrier gas flow rate of 4 mL/min. The inlet was operated at 200 °C, with a split ratio of 10:1 and a total flow rate of 47 mL/min. The TCD was operated at 220 °C with a reference flow of 24 mL/min and a makeup flow of 2 mL/min. The process variables were continuously monitored and recorded using Labview 2009.

One liter of Milli-Q water (≥18.2 mΩ cm) was charged into the reactor along with 0.25 g of photocatalyst (multifunctional catalysts) or variable amounts of photocatalyst and Pd catalyst (mixture approach). The reactor was sealed, the impeller was enabled (500 rpm), and the UV lamps were energized, which initiated the water-splitting reaction. Gas samples were taken automatically every 5 min during experiments, and the H_2 evolution was tracked by on line GC/TCD. An induction period was observed, typically 1−1.5 h in duration, depending on the catalyst formulation. Exposure of the photocatalyst to the reaction environment might have resulted in the modification of the catalyst and its catalytic properties. It is likely that, upon exposure to UV irradiation, photoexcited electrons were consumed by the catalyst material, partially reducing the photocatalyst during the induction period. After it had reached steady state, the reaction was monitored for an additional 2 h for accurate calculation of the H_2 evolution rate, after which 10 mL of aqueous CCl_4 stock solution (300 mg/L) was injected into the reactor using a gas-tight syringe to initiate the hydrodechlorination reaction.

Liquid samples (10 mL) were collected over a 2-h period. The samples were filtered with a 0.1-μm syringe filter (Sigma-Aldrich), transferred into the gas-tight sampling vials, diluted with Milli-Q water to the linear range of the calibration curves

dx.doi.org/10.1021/ie500344v | Ind. Eng. Chem. Res. 2014, 53, 9600−9607

for CCl_4 and $CHCl_3$, and transferred to 20 mL solid-phase microextraction (SPME) vials containing 2.0 g of NaCl. The samples were processed by solid-phase microextraction (SPME) followed by gas chromatography/mass spectrometry (GC/MS) analysis using an Agilent Technologies CTC Combipal autosampler (Sampler 80) and a GC/MS apparatus equipped with a 5975C VL mass-selective detector (MSD) and an HP-5MS (30 m × 0.250 mm × 0.25 μm) narrow-bore capillary column (Agilent J&W). The samples were incubated at 35 °C for 4 min at 500 rpm agitation. A preconditioned 23-gauge 50/30 μm DVB/CAR/PDMS SPME fiber assembly (Supelco) was used to extract the analytes from the liquid samples by the headspace method with 20 min of adsorption time prior to injection for a 0.75-min desorption time in splitless mode with an inlet temperature of 275 °C. The oven was held at 40 °C for 1.8 min and then ramped to 230 °C at 20 °C/min and held for 2 min. He (Praxair, LaserStar 5.5) was used as the carrier gas at a flow rate of 1 mL/min. The auxiliary line was maintained at 270 °C. The mass spectrometer scanned from 45 to 200 m/z. The mass spectra were collected in full-scan acquisition mode, whereas calibration and quantification of the analytes of interest were based on either selected-ion or full spectra. Calibration standards were run in triplicate with each set of reactor samples for analysis. One in five reactor samples was measured in duplicate. Blank samples were also run in the sequence.

A NiO/$NaTaO_3$:La catalyst known to be highly effective for photocatalytic water splitting in the UV range was selected as a basis for experimentation.[3,9] The catalysts were synthesized from the solid-state reaction of Ta_2O_5 (Sigma-Aldrich) with La_2O_3 (Sigma-Aldrich) and Na_2CO_3 (Sigma-Aldrich). The amounts were selected to give a nominal La loading of 1.4 wt %. The catalysts were calcined in air in a muffle furnace at 1170 K for 5 h in a Pt crucible, ground with a mortar and pestle, and then calcined in air at 1373 K for 15 h. NiO nanoparticles were dispersed on the catalyst by incipient wetness impregnation using $Ni(NO_3)_2{\cdot}6H_2O$ as a precursor and calcined in air at 217 °C for 8 h. The Ni and La loadings were subsequently determined by energy-dispersive X-ray fluorescence (EDXRF) spectroscopy using external standards composed of similar catalysts of known composition determined by inductively coupled plasma mass spectrometry (ICP-MS; Galbraith Laboratories, Knoxville, TN).

The NiO/$NaTaO_3$:La photocatalyst was further augmented to include Pd nanoparticles to effect the catalytic hydrodechlorination of CCl_4. Pd was dispersed onto the catalyst by incipient wetness impregnation using palladium(II) acetate (Sigma-Aldrich) as a precursor. The catalysts were calcined in air at 200 °C for 2 h and then reduced in H_2 for 3 h. The Pd loadings were ascertained by EDXRF spectroscopy using Rigaku RPF-SQX profile-fitting software. For the mixture-of-catalysts approach, the Ni loading of the photocatalyst was fixed at 0.16 wt % . A Pd−Au/IX ion-exchange resin catalyst (Rice University) composed of Pd decorated onto Au nanoparticles dispersed onto an ion-exchange resin support (Diaion SA 10A) was utilized to effect the catalytic hydrodechlorination of CCl_4 in the mixture-of-catalysts experiments.[10] The nanoparticles had a Pd-rich shell with about 60% surface coverage of Pd over a Au-rich core. The catalyst had an estimated assay of 0.00144 wt % Pd and 0.01 wt % Au. The Au nanoparticles are catalytically inert but promote hydrodechlorination reactions by inducing electronic and geometrical effects.[10,11] The Pd−Au/IX catalyst was reduced with H_2 for 2 h in Milli-Q water at room temperature under agitation prior to use in the photoreactor.

Select catalysts were analyzed by X-ray diffraction (XRD) using an Agilent SuperNova single-crystal diffractometer equipped with a microfocus Cu Kα radiation source (k = 1.54184 Å) and an Atlas CCD detector. The XRD data were processed with CrysAlisPro software (Agilent). The specific surface areas and pore size distributions of the optimized water-splitting catalyst and a multifunctional catalyst were ascertained by the multipoint Brunauer−Emmett−Teller (BET) and Barrett−Joyner−Halenda (BJH) adsorption models using nitrogen as the sorbate at 77 K with a Quantachrome Instruments 4200e Surface and Pore Analyzer. The catalysts were degassed for 3 h in helium at 60 °C prior to BET analysis. The multifunctional catalyst had 0.53 wt % Pd and 0.075 wt % Ni and was reduced in hydrogen at 100 °C.

A central composite design was employed to investigate the effects of the (nominal) Ni loading (0, 0.03, 0.075, 0.12, and 0.15 wt %), Pd loading (0.10, 0.28, 0.55, 0.82, and 1.00 wt %), and reduction temperature (100, 120, 150, 180, and 200 °C) on the rates of CCl_4 removal and H_2 evolution for a fixed initial CCl_4 concentration of 1.70 ± 0.187 ppm. In the mixture approach, a 2 × 2 factorial experiment with one center point investigating the effects of the catalyst amount on the H_2 evolution and CCl_4 removal rates was conducted using the Pd/Au/IX catalyst (W_2 = 10, 15, and 20 mL) and the NiO/$NaTaO_3$:La catalyst (W_1= 0.25, 0.50, and 0.75 g) for a fixed initial CCl_4 concentration of 1.03 ± 0.075 ppm. All experiments were conducted at 30 °C.

The reactor purge gas flow rate was fixed at 20 mL/min to avert mass-transfer limitations associated with H_2 evolution, while minimizing the stripping of CCl_4. Stripping experiments were conducted in the absence of UV and catalyst for various initial CCl_4 concentrations at a carrier gas flow rate of 20 mL/min and a stirring speed of 500 rpm. The CCl_4 concentration versus time in the reactor was monitored, and the data were used to account for the removal of CCl_4 by convective mass transfer. Control experiments were conducted with the reactor isolated with no carrier gas flow to assess the UV stability of CCl_4. The CCl_4 concentration was found to be invariant for 6 h of irradiation, confirming its stability. Control experiments assessing the photolytic degradation of dichloromethane and chloroform revealed that the photolysis rate constants were typically an order of magnitude greater than the stripping rate constant but an order of magnitude less than the rate constants for the catalytic hydrodechlorination of CCl_4 for the multi-functional catalyst approach. The first-order rate constants for the stripping and photolytic degradation of chloroform and dichloromethane are outlined in Table S1 (see the Supporting Information). Control experiments were also conducted in the absence of UV irradiation but in the presence of the catalysts to assess removal of CCl_4 by adsorption, which was found to be negligible on the low-specific-surface-area photocatalysts, as well as on the Pd/Au/IX catalyst. In a separate set of experiments in an essentially identical apparatus, control experiments were conducted where the CCl_4 concentration was monitored with and without UV irradiation in the presence of inert carrier gas flow and with and without a NiO/$NaTaO_3$:La water-splitting photocatalyst (0.2 wt % NiO and 2 mol % La), which confirmed that the water-splitting photocatalyst was not active for CCl_4 removal.[4]

dx.doi.org/10.1021/ie500344v | Ind. Eng. Chem. Res. 2014, 53, 9600−9607

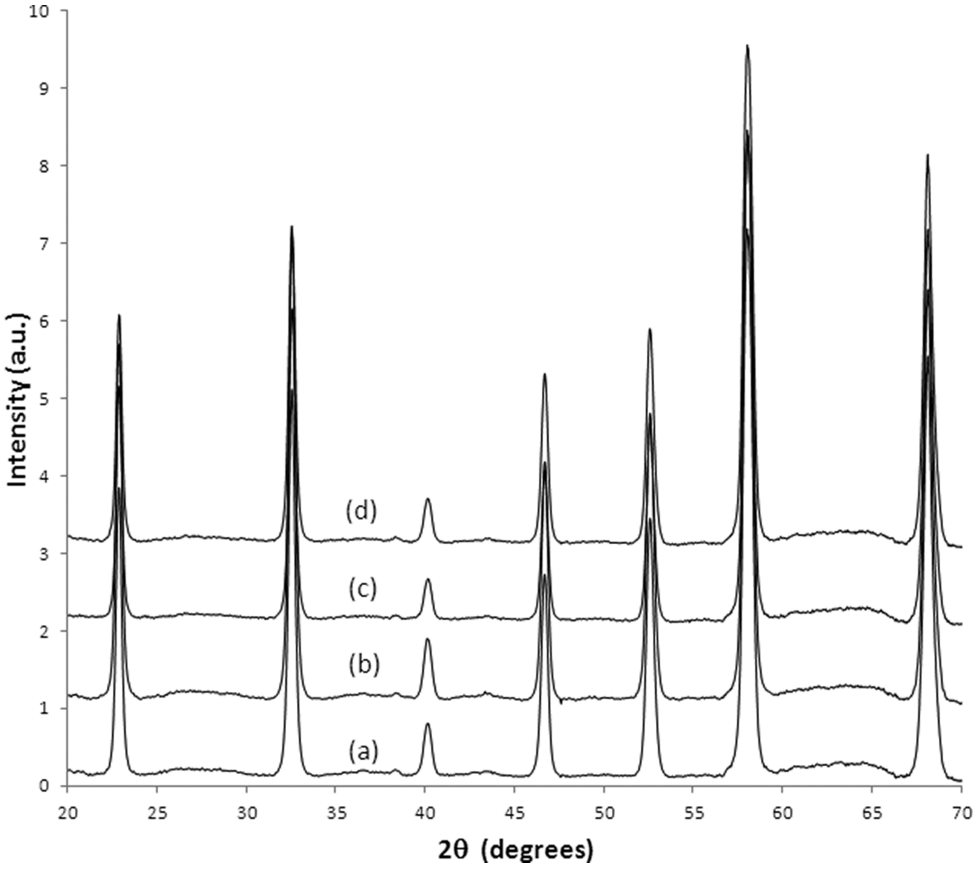

Figure 1. XRD spectra of select catalysts: (a) $NaTaO_3$:La, (b) NiO/$NaTaO_3$:La [0.16 wt % Ni], (c) Pd−NiO/$NaTaO_3$:La (0.53 wt % Pd, 0.06 wt % Ni), (d) Pd−NiO/$NaTaO_3$:La (0.76 wt % Pd, 0.02 wt % Ni).

RESULTS AND DISCUSSION

The XRD patterns of La-doped $NaTaO_3$, NiO/$NaTaO_3$:La, and Pd−NiO/$NaTaO_3$:La catalysts are presented in Figure 1. All samples are exactly indexed as the pure $NaTaO_3$ orthorhombic structure.[12] In contrast, others have reported impurity phases such as Ta_2O_5 formed as a result of an insufficient crystallization during the synthesis.[13] The results in Figure 1 suggest that lanthanum was uniformly incorporated into the $NaTaO_3$ lattice. In addition, diffraction peaks associated with NiO and Pd crystallites are not evident from either the Pd−NiO/$NaTaO_3$:La or NiO/$NaTaO_3$:La catalyst. From this observation, it can be inferred that the NiO and Pd crystallites were highly dispersed on the surface.[14] The characterization of the specific surface area and pore size distributions for the optimized water-splitting catalyst NiO/$NaTaO_3$:La and Pd−NiO/$NaTaO_3$:La multifunctional catalyst are presented in Table S2 (Supporting Information). As expected, the photocatalyst has a relatively low surface area, slightly lower than the ca. 3 m^2/g reported originally by Kato et al.[9] It can be concluded from the data in Table S2 (Supporting Information) that the augmentation of the photocatalyst with Pd resulted in a slight loss of specific surface area and total pore volume.

The kinetic data were reconciled to account for the stripping of CCl_4 by the purge gas. The CCl_4 concentration (C_A) versus time data for the stripping experiment exhibited first-order kinetics and was fit to a two-parameter empirical model (eq 1) using NLREG (version 6.5, Sherrod Software) with good agreement (R^2 = 0.996, F = 2040). The stripping constant, k_s, was found to be 0.00758 min^{-1}. The CCl_4 concentration versus time plots also exhibited first-order kinetics for the catalytic reactions. The data from each experiment were fit to an exponential empirical model as in eq 1, also with very good agreement, typically with $R^2 \geq 0.99$, giving the apparent reaction rate constant k' and the initial concentration C_{A0} (μmol/L). The reconciled first-order rate constant, k, was obtained by solving eq 2 and used to calculate the initial CCl_4 reaction rate [μmol/(L min)]. The turnover frequency was calculated based on the initial reaction rate and the number of Pd atoms present in the catalyst.[10]

$$C_A(t) = C_{A0} \exp(-k_s t) \quad (1)$$

$$-\frac{dC_A}{dt} = k_s C_A + k C_A = k' C_A \quad (2)$$

The results of the mixture-approach experiments (Figure 2, Table 1) suggest a photocatalyst limitation as evidenced by the significant decrease in the specific H_2 evolution activity with increasing photocatalyst mass, which indicates that the photocatalyst was irradiated less efficiently with increasing slurry density. Changes in the amount of ion-exchange resin impacted neither the photocatalyst performance nor the estimate of the rate constant. However, the normalized rate constant for CCl_4 removal and the initial specific reaction rate diminished with increasing amount of photocatalyst, despite the increase in the hydrogen evolution rate with increasing photocatalyst mass, suggesting that the presence of the photocatalyst adversely impacted the performance of the ion-exchange resin catalyst. Significantly, the results of the mixture-approach experiments demonstrate the proof of concept of the

dx.doi.org/10.1021/ie500344v | Ind. Eng. Chem. Res. 2014, 53, 9600−9607

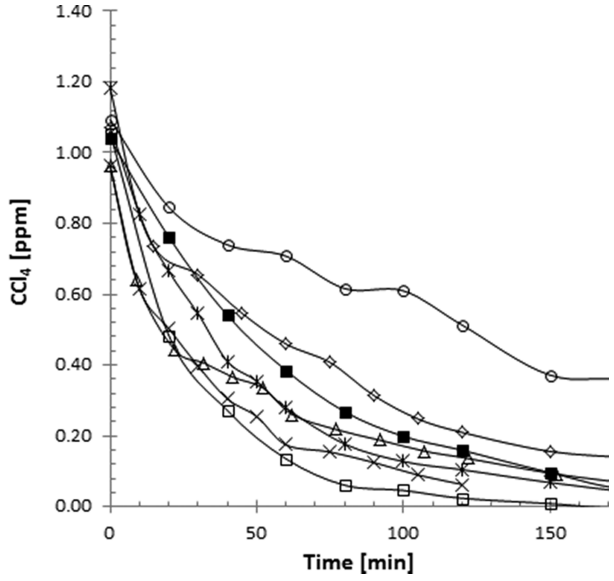

Figure 2. CCl_4 concentration (ppm) versus time profiles for the experiments from the mixture-of-catalysts approach DoE. (○) Control experiment (no UV, no catalyst), (■) trial 1, (◊) trial 2, (*) trial 3, (Δ) trial 4, (□) trial 5a, and (×) trial 5b.

Table 1. Results of the Mixture-of-Catalysts Approach Experiments

trial ID	W_1[a] (g)	W_2[b] (mL)	k [L/(min mL)]	initial rate [μmol/(L min mL)]	H_2[c] (mmol h)
1	0.251	10	0.00886	0.00601	0.885
2	0.751	10	0.00570	0.00372	1.65
3	0.501	15	0.0165	0.00806	1.10
4	0.752	20	0.0116	0.00318	1.44
5a	0.253	20	0.0278	0.00947	0.850
5b[d]	0.252	20	0.0208	0.00617	0.828

[a]Mass of 0.15 wt % $NiO/NaTaO_3$:La catalyst. [b]Volume of Pd−Au/IX resin catalyst swelled in Milli-Q water. [c]Steady-state H_2 evolution measured before injection of CCl_4. [d]All regression analysis was based on the first 2 h of data collected, except for repeated experiment 5b, for which the first 60 min of data were used to obtain regression model; NLREG did not converge to a solution when the full data set was used.

catalytic technology, specifically that the H_2 produced in situ from water splitting can be utilized to effect the catalytic reduction of a trace contaminant in aqueous medium, as evidenced by the significant and measurable catalytic conversion of CCl_4 accompanied by the detection of the hydrodechlorination products chloroform and dichloromethane by GC/MS National Institute of Standards and Technology (NIST) library matching.

In stark contrast, the multifunctional catalysts resulted in the rapid removal of CCl_4 with conversions as high as 90% and 95% in 5 and 10 min, respectively (Figure 3). The rate constants for the catalytic hydrodechlorination of CCl_4 were found to be 2 orders of magnitude greater than the stripping constant (Table S3, Supporting Information). Chloroform and trace dichloromethane were identified in the product as intermediates by NIST spectral library match, confirming the hydrodechlorination pathway. Methane was detected by GC/TCD in the reactor gas effluent in a preliminary experiment with an initial CCl_4 concentration of ca. 300 ppm (Figure S1), further demonstrating the hydrodechlorination pathway. In comparison, the mixture-of-catalysts approach required a

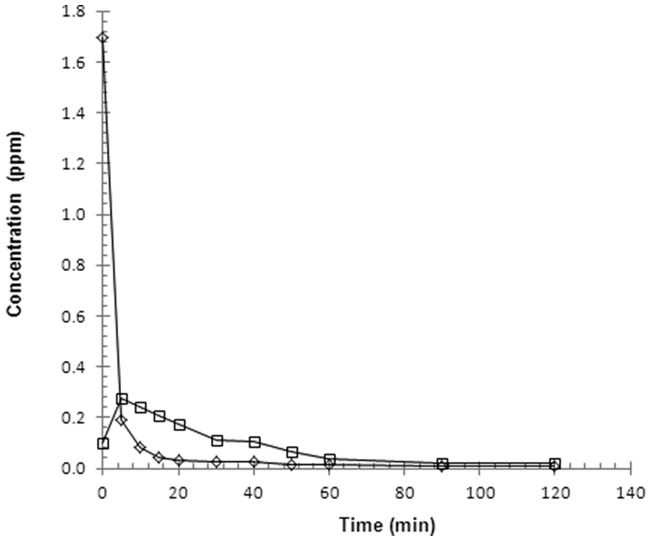

Figure 3. (◊) CCl_4 and (□) $CHCl_3$ concentration (ppm) versus time profiles for a representative experiment from the multifuncitonal catalyst approach DoE (0.53 wt % Pd, 0.06 wt % Ni, T_{red} = 100 °C).

minimum of 1.5 h to achieve 95% conversion, and in some cases, 95% conversion could not be achieved even after 5 h of reaction. It is evident from Figure 3 that chloroform is an intermediate product undergoing further reaction. The nonzero chloroform concentration at time zero was due to uncertainty in the measurements. The first liquid sample was, in fact, taken about 1 min after CCl_4 injection after the syringe had been purged, which provided sufficient time to produce a substantial amount of chloroform. Significantly, although CCl_4 cannot be photolytically degraded, the products of the hydrodechlorination reaction, chloroform and dichloromethane, can be readily photolyzed in addition to possible further degradation by hydrodechlorination. Thus, the photocatalytic reduction of CCl_4 in the presence of UV radiation opens up alternative pathways for the removal of the hydrodechlorination by-products.

Analysis of variance (ANOVA) and response surface modeling exploring the effects of the Pd and Ni loadings and catalyst reduction temperature on the initial CCl_4 reaction rates and turnover frequencies were conducted using JMP 8 (SAS). The results of the ANOVA are given in Table S4 (Supporting Information), and select projections of the response hypersurfaces are given in Figure 4. All three synthesis parameters investigated had significant and highly nonlinear effects on the CCl_4 reaction rates. The catalyst activity was strongly dependent on the Pd loading. A locally optimum combination of 0.19 wt % Ni and 0.46 wt % Pd with a reduction temperature of 100 °C maximized the reaction rate. Therefore, both the NiO nanoparticles and the Pd sites are important in the photocatalytic hydrodechlorination of CCl_4. The experiment with 0 wt % Ni resulted in H_2 evolution and the effective removal of CCl_4, albeit at a below-average rate, which shows that the Pd sites alone are sufficient to effect the photocatalytic hydrodechlorination of CCl_4. However, the addition of NiO generally had a positive impact on catalyst activity, except at high catalyst reduction temperatures, for which increases in both Pd and Ni mass fractions had adverse effects on catalyst activity.

The reduction temperature had a profound effect on the catalyst activity. The combined effects of catalyst reduction

dx.doi.org/10.1021/ie500344v | Ind. Eng. Chem. Res. 2014, 53, 9600−9607

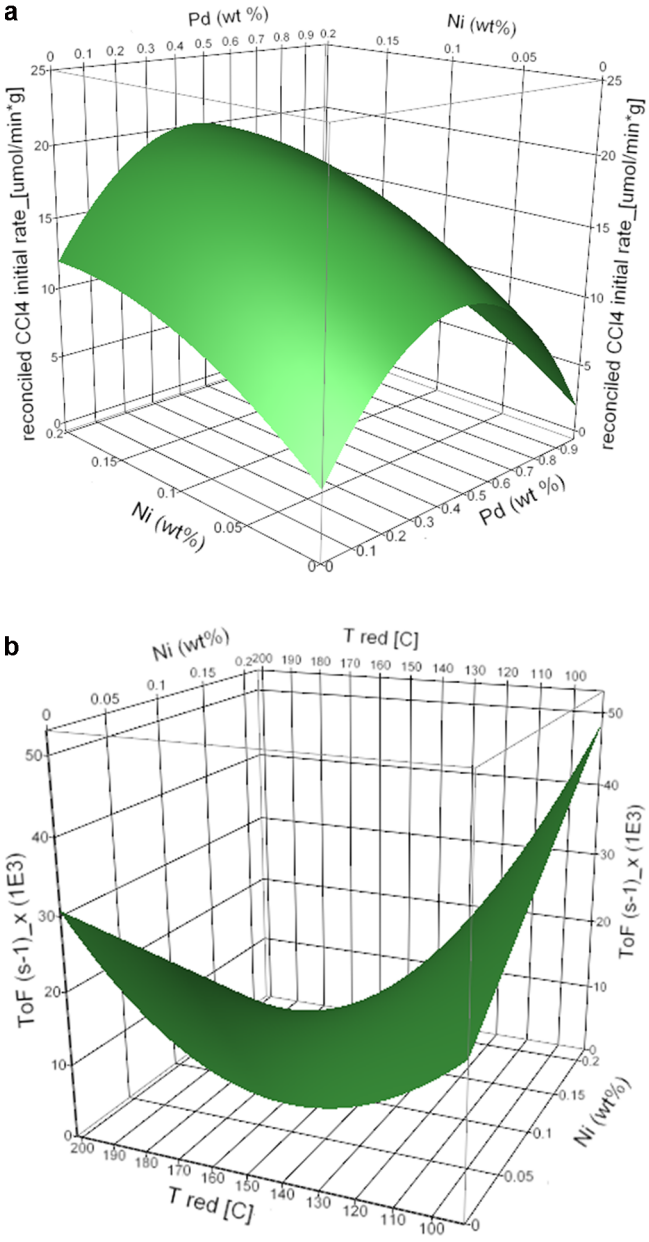

Figure 4. (a) Effects of Ni and Pd loadings (wt %) on the initial rate of reaction at T_{red} = 100 °C. (b) Effects of Ni loading and catalyst reduction temperature on the turnover frequency at 0.46 wt % Pd.

temperature and Ni and Pd loadings on the catalyst activity for CCl_4 removal resulted in saddle-shaped response surfaces with the greatest catalytic activity favored at lower catalyst reduction temperatures. It is hypothesized that the major effect of the catalyst reduction temperature on the catalyst activity is likely due to its influence on the Pd crystallite size and dispersion, which implies that the reaction is structure-sensitive. The significant two-way interaction between the Ni loading and the reduction temperature can be interpreted to mean that the effect of the catalyst reduction temperature on the catalyst activity is dependent on the Ni loading, which might suggest that the presence of NiO nanoparticles improves the dispersion of the Pd crystallites or results in some other geometrical or electronic effect. The effects of the Pd and Ni loadings and the catalyst reduction temperature on the resultant catalyst turnover frequency gave a similar result. A local maximum in the turnover frequency was found for 0.1 wt % Pd, 0.19 wt % Ni, and 100 °C reduction temperature. Thus, the atomic efficiency was the greatest for the lowest Pd loading, the lowest catalyst reduction temperature, and the maximum surface concentration of NiO, which suggests a highly dispersed Pd-on-NiO catalyst giving rise to optimal performance. However, detailed catalyst characterization including high-resolution transmission electron microscopy (HRTEM) analysis is needed to confirm the effects of the catalyst parameters on the crystallite size and dispersion, as well as to fully elucidate the structure of the active sites.

The addition of Pd to the photocatalyst suppressed the H_2 evolution rate by 3 orders of magnitude, likely as a result of recombination sites introduced by the Pd crystallites. The Pd loading was the only variable that significantly affected the H_2 evolution activity, which diminished nonlinearly with increasing Pd mass fraction. The introduction of CCl_4 into the reactor resulted in an increase in the net H_2 evolution rate by a factor of about 2−4 in all multifunctional catalyst experiments, predominantly correlating with the Pd loading and the catalyst reduction temperature, whereas the Ni loading had a marginally significant effect. A plausible explanation for the increase in H_2 evolution is that competition for H_2 from the hydrodechlorination reaction and the competitive adsorption introduced by the presence of CCl_4 and its reaction products changes the relative surface concentrations of adsorbed species, suppressing the recombination of H_2 and O_2 and thereby increasing the H_2 and O_2 evolution rates.

It is evident that CCl_4 was more rapidly converted by the multifunctional catalyst approach. Control experiments demonstrated that the $NiO/NaTaO_3$:La photocatalyst is not active for the hydrodechlorination reaction.[4] Therefore, the high activity of the multifunctional catalyst arose upon augmentation of the photocatalyst with Pd and is attributed to the presence of both Pd and NiO sites. There are a several plausible explanations for the apparent effects of these catalyst parameters on the activity for the hydrodechlorination (HDC) reaction, as well as the significant kinetic enhancement afforded by the multifunctional catalyst approach compared to the mixture-of-catalysts approach. It is possible that NiO nanoparticles might have promoted the reaction by assisting the dispersion of the Pd crystallites, by inducing some other geometrical or electronic effect, or by providing H_2 evolution sites in close proximity to the catalytic hydrodechlorination sites. In the multifunctional catalyst approach, H_2 is created on the photocatalyst surface at or near Pd active sites for the hydrodechlorination of CCl_4, thus obviating the internal and external mass-transfer limitations introduced in the mixture-of-catalysts approach. Another possibility is that the presence of Pd in contact with the semiconductor might have enabled alternative reaction mechanisms not available on the conventional hydrodechlorination catalyst, which enhanced the reaction rate. For example, CCl_4 might have reacted directly with photoexcited electrons, resulting in its decomposition by two-electron-transfer processes.[6] Finally, the phenomena associated with plasmonic photocatalysis and the Schottky junction created by the noble metal dispersed on the semiconductor photocatalyst might have modified the electronic properties of the Pd crystallites in a manner that significantly enhanced the hydrodechlorination of CCl_4.[15] However, if so, the photocatalytic reaction was not enhanced.

dx.doi.org/10.1021/ie500344v | Ind. Eng. Chem. Res. 2014, 53, 9600−9607

CONCLUSIONS

The technical feasibility of the photocatalytic hydrodechlorination of CCl_4 was realized utilizing a multifunctional Pd/NiO/$NaTaO_3$:La catalyst and a mixture approach with an optimized NiO/$NaTaO_3$:La water-splitting catalyst and Pd−Au/IX hydrodechlorination catalyst. The latter approach, in which the water-splitting and hydrodechlorination steps were decoupled, demonstrated the proof of concept that micropollutants in water can be effectively removed by direct reaction with H_2 produced in situ from photocatalytic water splitting. Chloroform and dichloromethane were observed as intermediate species in the liquid samples in all experiments, confirming the hydrodechlorination pathway. Augmentation of the NiO/$NaTaO_3$:La catalyst with Pd resulted in a loss in H_2 evolution activity by 3 orders of magnitude, likely due to the introduction of recombination sites by the Pd crystallites. However, the Pd/NiO/$NaTaO_3$:La multifunctional catalyst showed a remarkable catalytic activity for the hydrodechlorination of CCl_4 and utilized the H_2 far more efficiently than the mixture approach. The Pd and Ni loadings and the catalyst reduction temperature had significant nonlinear effects on the catalyst activity for CCl_4 removal, indicating that both NiO and Pd sites play important roles in the hydrodechlorination reaction. The significant effects of the Pd loading and catalyst reduction temperature on the turnover frequency are likely due to their influence on the Pd crystallite size and dispersion, which implies that the reaction is structure-sensitive.

ASSOCIATED CONTENT

Supporting Information

Results of the control experiments assessing stripping and photolytic degradation of CCl_4, $CHCl_3$, and CH_2Cl_2 (Table S1). Results of specific surface area and pore size distribution analyses (Table S2). Results of multifunctional catalyst experiments (Table S3). ANOVA results for multifunctional catalyst experiments (Table S4). Peak area assigned to methane (retention time 2.1 min) as a function of time on stream obtained by online GC/TCD analysis during the photocatalytic reduction of carbon tetrachloride using a Pt/$NaTaO_3$:La multifunctional catalyst (Figure S1). This material is available free of charge via the Internet at http://pubs.acs.org.

AUTHOR INFORMATION

Corresponding Author

*E-mail: bokeefe@trojanuv.com.

Author Contributions

The manuscript was written through the contributions of all authors. All authors have given approval to the final version of the manuscript.

Notes

The authors declare the following competing financial interest(s): Trojan Technologies is seeking patent protection related to some of the general concepts surrounding the subject matter of this manuscript. However, neither the authors nor Trojan Technologies will profit financially from the publication of this manuscript.

ACKNOWLEDGMENTS

The Pd−Au/IX hydrodechlorination catalyst was prepared by Mr. Zhun Zhao (Rice University). The UV source was characterized by Dr. Jim Robinson, Dr. Tina Liu, and Ms. Farnaz Daynouri-Pancino. XRD analysis was conducted by Professor Dmitriy Soldatov. BET analysis was conducted by Mr. Jay Leitch. Mr. Atif Vaniyambadi and Ms. Winnie Lau assisted with the operation of the photoreactor and sample collection. Funding for Y.L. was provided by the MITACS Accelerate program, Government of Canada.

ABBREVIATIONS

ANOVA = analysis of variance
C_{A0} = initial concentration of carbon tetrachloride
CCl_4 = carbon tetrachloride
CH_2Cl_2 = dichloromethane
$CHCl_3$ = chloroform
DoE = design of experiment
e^- = electron
h^+ = hole
H^+ = proton
HDC = hydrodechlorination
IX = ion-exchange resin catalyst
ppm = parts per million
R = micropollutant to be catalytically converted
R^- = product of the reaction of micropollutant R with donated electron from photocatalyst
R′ = product of the reaction of micropollutant with hydrogen
T_{red} = reduction temperature
UV = ultraviolet
W = catalyst mass (g) charged to the reactor

REFERENCES

(1) Hot Issues: Water Scarcity, FAO, 2013, http://www.fao.org/nr/water/issues/scarcity.html (accessed Sep 9, 2013).

(2) O'Keefe, W. K. Sasges, M. R. (Trojan Technologies). Photocatalyst Composition of Matter. World Patent WO 2011/106864, 2011.

(3) Kudo, A.; Maseki, Y. Heterogeneous Photocatalyst Materials for Water Splitting. *Chem. Soc. Rev.* **2009**, *38* (1), 253.

(4) Fu, H. Study on the Photocatalytic Purification of Chlorinated Organic Contaminants in Water. M.Sc. Thesis, University of Tokyo, Tokyo, Japan, 2012; pp 49−50.

(5) Stark, J.; Rabani, J. Photocatalytic Dechlorination of Carbon Tetrachloride Solutions in TiO_2 Layer Systems: A Chain Reaction Mechanism. *J. Phys. Chem. B* **1999**, *103*, 8524.

(6) Chien, Y. C.; Wang, H. P.; Liu, S. H.; Hsiung, T. L.; Tai, H. S.; Peng, C. Y. Photocatalytic Decomposition of CCl_4 on Zr-MCM-41. *J. Hazard. Mater.* **2008**, *151*, 461.

(7) Yao, Z.; Wang, M.; Sun, S.; Jia, R.; Li, H. High Performance Photocatalysts based on N-Doped Graphene P-25 for Photocatalytic Reduction of Carbon Tetrachloride. *J. Inorg. Organomet. Polym.* **2014**, *24*, 315.

(8) Hsiao, C. Y.; Lee, C. L.; Ollis, D. F. Heterogeneous Photocatalysis: Degradation of Dilute Solutions of Dichlormethane (CH_2Cl_2), Chloroform ($CHCl_3$) and Carbon Tetrachloride (CCl_4) with Illuminated TiO_2 Photocatalyst. *J. Catal.* **1983**, *82*, 418.

(9) Kato, H.; Asakura, K.; Kudo, A. Highly Efficient Water Splitting into H_2 and O_2 over Lanthanum Doped $NaTaO_3$ Photocatalysts with High Crystallinity and Surface Nanostructure. *J. Am. Chem. Soc.* **2003**, *125* (10), 3082.

(10) Wong, M. S.; Alvarez, P. J. J.; Fang, Y. I.; Akcin, M.; Nutt, M. O.; Miller, J. T.; Heck, K. N. Cleaner Water Using Bimetallic Nanoparticle Catalysts. *J. Chem. Technol. Biotechnol.* **2008**, *84* (2), 158.

(11) Velazquez, J. C.; Leekumjorn, S.; Nguyen, Q. X.; Fang, Y. L.; Heck, K. N.; Hopkins, G. D.; Reinhard, M.; Wong, M. S. Chloroform Hydrodechlorination Behaviour of Alumina-Supported Pd and PdAu Catalysts. *AIChE. J.* **2013**, *59*, 12.

(12) Husin, H.; Chen, M. H.; Su, W. N.; Pan, C. J.; Chuang, W. T.; Sheu, H. S.; Hwang, B. J. Green Fabrication of La-Doped $NaTaO_3$ via

H_2O_2 Assisted Sol−Gel Route for Photocatalytic Hydrogen Production. *Appl. Catal. B* **2011**, *102*, 343.
(13) Li, X.; Zhang, J. Facile Hydrothermal Synthesis of Sodium Tantalate ($NaTaO_3$) Nanocubes and High Photocatalytic Properties. *J. Phys. Chem. C* **2009**, *113*, 19411.
(14) Hu, C. C.; Teng, H. Structural Features of p-Type Semiconducting NiO as a Co-Catalyst for Photocatalytic Water Splitting. *J. Catal.* **2010**, *272*, 1.
(15) Zhang, X.; Chen, Y. L.; Liu, R. S.; Tsai, D. P. Plasmonic photocatalysis. *Rep. Prog. Phys.* **2013**, *76*, 41.